Iraqi Journal of Physics, 2022 *Vol.20, No.4, PP.18-27*

DOI: 10.30723/ijp.v20i4.1013

P-ISSN: 2070-4003
E-ISSN: 2664-5548

Elastic Form Factors and Matter Density Distributions of Some Neutron-Rich Nuclei

Hawraa K. Mahdi[1a*] and Ahmed N. Abdullah[1b]

Department of Physics, College of Science, University of Baghdad, Baghdad, Iraq

[b]E-mail: ahmed.n@sc.uobaghdad.edu.iq

[a*]Corresponding author: hawraa.kadim1204a@sc.uobaghdad.edu.iq

Abstract

The ground-state properties of exotic ^{18}N and ^{20}F nuclei, including the neutron, proton and matter densities and related rms radii are investigated using the two-body model of [Core + n] within Gaussian (GS) and Woods Saxon (WS) wave functions. The long tail is evident in the computed neutron and matter densities of these nuclei. The plane wave Born approximation (PWBA) is used to calculate the elastic form factors of these exotic nuclei. The variation in the proton density distributions due to the presence of the extra neutrons in ^{18}N and ^{20}F leads to a major difference between the elastic form factors of these exotic nuclei and their stable isotopes ^{14}N and ^{19}F. The reaction cross sections for these nuclei are investigated using the Kox and Glauber models. Furthermore, the Glauber model is employed to calculate the matter rms radii of these exotic nuclei. The calculated results for the selected exotic nuclei are in a good agreement with the experimental data.

Article Info.

Keywords:
Neutron rich-nuclei, Halo nuclei, Exotic nuclei, Two-body model, Kox formula.

Article history:
Received: Jun. 22, 2022
Accepted: Sep. 15, 2022
Published: Dec.01, 2022

1. Introduction

Due to their exotic properties, studying exotic (halo) nuclear structures at the proton and neutron drip lines has become a hot subject in modern nuclear physics [1-5]. The halo effect is caused by the last few nucleons' low separation energy and occupation of states with ℓ =0,1 which allows the halo nucleon wave functions to extend to large matter radii [6]. Studying the halo structure is very useful for understanding the nuclear structure in both theories and experiments. Because halo nuclei have a short lifetime, they should be investigated by radioactive beam facilities [7]. Few body models can be used to represent the halo nuclei, which are considered to be produced by coupling a compact core with a few weakly bound nucleons. As a result, the halo systems can be divided into two types: the two-body system, in which one valence nucleon surrounds the nucleus core, likely the one neutron halo ^{19}C; and the three-body halo, in which two valence nucleons surround the nucleus core, likely the two-neutron halo ^{14}Be [8].

Abdullah [9] investigated the ground state in the (^{6}He, ^{11}Li, ^{12}Be, and ^{14}Be) halo nuclei using a three-body model (Core + 2n). The neutron density and predicted matter density for these nuclei demonstrate the characteristics of the long tail. The computed values for the density of matter were in good agreement with the experiment results. Abdullah [10] has investigated the ground state features such as the proton, neutron, and matter densities and the rms nuclear radii of unstable neutron-rich ^{14}B, ^{15}C, ^{19}C, and ^{22}N nuclei using the cosh potential radial wave functions within the two-body model of (Core + n). The obtained results showed that the cosh potential radial wave functions of the two-body model are capable of reproducing neutron halo in these nuclei.

In this work, the Gaussian (GS) and Woods-Saxon (WS) wave functions within the two-body model (TBM) of $[\mathrm{Core} + \mathrm{n}]$ were used to investigate the properties of the ground state for exotic ^{18}N and ^{20}F nuclei, including the neutron, proton and matter densities, and the corresponding rms radii and elastic form factors. The Kox and Glauber models were used to investigate the reaction cross-sections (σ_R) for these nuclei.

2. Theory

The matter density $\rho_m(r)$ of halo nuclei can be obtained by adding the core density $\rho_c(r)$ and the valence density $\rho_v(r)$ [11]:

$$\rho_m(r) = \rho_c(r) + \rho_v(r) \tag{1}$$

The GS and WS techniques were employed in this investigation. Both core and valence densities in the GS technique are described by the Gaussian wave functions [11]:

$$\rho_c(r) = A_c \frac{1}{(\sqrt{\pi} a_c)^3} e^{-r^2/a_c^2} \tag{2}$$

$$\rho_v(r) = A_v \frac{1}{(\sqrt{\pi} a_v)^3} e^{-r^2/a_v^2} \tag{3}$$

$$\rho_m(r) = A_c\, G^3(a_c, r) + A_v\, G^3(a_v, r) \tag{4}$$

$$G^3(a_g, r) = \frac{1}{(\sqrt{\pi} a_g)^3} e^{-r^2/a_g^2}\ ; \quad g \equiv c, v \tag{5}$$

where $G^{(3)}$ is the Gaussian function;

$$\int G^{(3)}(a_g, r) d\vec{r} = 1 \tag{6}$$

In the WS technique, both core and valence densities are described by the WS radial wave functions obtained from the radial part solution of the Schrödinger equation with WS potential [12]:

$$\frac{\hbar^2}{2m} \frac{d^2 R_{n\ell j}(r)}{dr^2} + \left[\varepsilon_{n\ell j} - V(r) - \frac{\hbar^2}{2m} \frac{\ell(\ell+1)}{r^2}\right] R_{n\ell j}(r) = 0 \tag{7}$$

where: m, $\varepsilon_{n\ell j}$ and $V(r)$ are the reduced mass, single-particle binding energy (ε) and the core potential, respectively. $V(r)$ can be written as [9]:

$$V(r) = V_0(r) + V_{so}(r)\, L.S + V_c(r) \tag{8}$$

where $V_0(r)$, $V_{so}(r)$ and $V_c(r)$ are the central, spin-orbit and Coulomb (for protons only) potentials, respectively, which take the following forms [9]:

$$V_0(r) = \frac{-V_0}{1+\left[e^{(r-R_0)/a_0}\right]} \tag{9}$$

$$V_{so}(r) = V_{so} \frac{1}{r} \left[\frac{d}{dr} \frac{1}{\left(1+e^{(r-R_{so})/a_{so}}\right)}\right] \tag{10}$$

$$V_c(r) = \begin{cases} \frac{Ze^2}{r} & \text{for} \quad r > R_c \\ \frac{Ze^2}{R_c}\left[\frac{3}{2} - \frac{r^2}{2R_c^2}\right] & \text{for} \quad r \leq R_c \end{cases} \quad \textbf{(11)}$$

$V_c(r) = 0$ for neutrons.
$\rho_m(r)$ in Eq.(1) can be written in terms of neutron $\rho_n(r)$ and proton $\rho_p(r)$ densities [13]:

$$\rho_m(r) = \rho_n(r) + \rho_p(r) \quad \textbf{(12)}$$

where

$$\rho_n(r) = \rho_n^c(r) + \rho_n^v(r) \quad \textbf{(13)}$$
$$\rho_p(r) = \rho_p^c(r) + \rho_p^v(r) \quad \textbf{(14)}$$

where $\rho_n^c(r)\left(\rho_p^c(r)\right)$ and $\rho_n^v(r)\left(\rho_p^v(r)\right)$ are the core and valence neutron (proton) densities, respectively. The neutron (r_n), proton $\left(r_p\right)$, core (r_c) and matter (r_m) rms radii are given by [9]:

$$r_g = \langle r_g^2 \rangle^{1/2} = \left[\frac{\int r^2 \rho_g(r) dr}{\int \rho_g(r) dr}\right]^{1/2} \qquad g = n, p, c, m \quad \textbf{(15)}$$

The elastic form factor is given as [14]:

$$F(q) = \frac{4\pi}{Z}\int_0^\infty \rho_p(r) j_0(qr) r^2 dr \quad \textbf{(16)}$$

The Kox and Glauber models have been used to investigate the reaction cross sections for these nuclei. The σ_R in the framework of the Glauber model is given as [15]:

$$\sigma_R = 2\pi \int [1 - T(b)] b\, db \left(1 - \frac{B_c}{E_{cm}}\right), \quad \textbf{(17)}$$

where T(b) is the transparency function. In the Optical Limit Approximation (OLA), the T(b) is written as [16]:

$$T(b) = \left|S_{el}^{OL}(b)\right|^2 \quad \textbf{(18)}$$
$$S_{el}^{OL}(b) = \exp[iO_{PT}(b)] \quad \textbf{(19)}$$
$$O_{PT}(b) = \int_{-\infty}^{\infty} dR_3 \int dr_1 \int dr_2 \rho_P(r_1) \rho_T(r_2) f_{NN}(|R + r_1 - r_2|) \quad \textbf{(20)}$$

The σ_R in the framework of the Kox model is given as [17]:

$$\sigma_R(E) = \pi r_0^2 \left(A_p^{1/3} + A_t^{1/3} + a \frac{A_p^{1/3} A_t^{1/3}}{(A_p^{1/3} + A_t^{1/3}} - C(E) \right)^2 \left(1 - \frac{B_c}{E_{cm}}\right) \quad \textbf{(21)}$$

3. Results and Discussion

The GS and WS wave functions within the TBM of $[\mathrm{Core} + \mathrm{n}]$ were utilized to investigate the ground-state characteristics of exotic ^{18}N (S_n=2.828 MeV, $\tau_{1/2}$=619.2 ms) and ^{20}F (S_n=6.601MeV, $\tau_{1/2}$=11.163s [18,19] nuclei, including $\rho_n(r)$, $\rho_p(r)$ and $\rho_m(r)$ distributions, related rms radii and elastic form factors. σ_R for these nuclei was investigated using the Kox formula and OLA of GM with the single-particle HO wave functions.

The analysis was performed assuming ^{17}N (J^π, T=1/2$^-$, 3/2) and ^{19}F (J^π, T=1/2$^+$, 1/2) cores plus one valence proton structure for ^{18}N (J^π, T=1$^-$, 2) and ^{20}F (J^π, T=2$^+$,1), consecutively. The core and valence densities in the GS technique were described by the Gaussian functions. In the WS technique, both core and valence densities were described by the WS radial wave functions. The configurations of the ^{17}N and ^{19}F core nuclei are:

$$\{(1s_{1/2})^4, \left(1p_{\frac{3}{2}}\right)^8, \left(1p_{\frac{1}{2}}\right)^3, (1d_{5/2})^2\}$$

and

$$\{(1s_{1/2})^4, \left(1p_{\frac{3}{2}}\right)^8, \left(1p_{\frac{1}{2}}\right)^4, (1d_{5/2})^3\}$$

consecutively. It was assumed that the valence neutron of both ^{18}N and ^{20}F occupied the $2s_{1/2}$ orbit.

Table 1 displays the WS parameters and GS size parameters (a_c, a_v) used in the present work. Tables 2 and 3 present the calculated and experimental results of $r_n, r_p, r_c,$ and r_m for the exotic ^{18}N and ^{20}F nuclei. The calculated ε for the selected exotic nuclei is displayed in Table 4.

Table 1: The WS parameters and GS size parameters.

Nuclei	V_0 (MeV)		V_{so} (MeV)	$a_0 = a_{so}$ (fm)	$r_0 = r_{so}$ (fm)	r_c (fm)	a(fm)	
	Core	Valence					a_c	a_v
^{18}N	62.532	44.260	6.0	0.742	1.296	1.399	2.03	4.15
^{20}F	58.137	42.110	6.0	0.532	1.286	1.386	2.09	4.57
^{14}N	70.962		6.0	0.715	1.319	1.431	2.017	
^{19}F	62.515		6.0	0.538	1.282	1.392	1.758	

Table 2: The calculated r_p and r_n for ^{18}N and ^{20}F.

Nuclei	$\langle r_p^2\rangle^{1/2}$		$\langle r_n^2\rangle^{1/2}$		$\langle r_n^2\rangle^{1/2}_{exp}$ [20]
	GS	WS	GS	WS	
^{18}N	2.48	2.54	2.92	2.91	2.89 ± 0.04
^{20}F	2.61	2.63	2.98	2.96	2.90 ± 0.06

Table 3: The calculated r_c and r_m for ^{18}N and ^{20}F.

Nuclei	$\langle r_c^2\rangle^{1/2}$		$\langle r_c^2\rangle^{1/2}_{exp}$ [20]	$\langle r_m^2\rangle^{1/2}$		$\langle r_m^2\rangle^{1/2}_{exp}$ [21]
	GS	WS		GS	WS	
^{18}N	2.48	2.50	2.49 ± 0.15	2.69	2.71	2.69 ± 0.05
^{20}F	2.61	2.65	2.61 ± 0.07	2.82	2.82	2.79 ± 0.03

Table 4: The calculated ε for the selected halo nuclei.

Nucleus	$n\ell_j$	Proton	Neutron
		ε_{cal} (MeV)	ε_{cal} (MeV)
^{18}N	$1s_{1/2}$	37.798	40.965
	$1p_{3/2}$	23.037	25.975
	$1p_{1/2}$	22.475	25.406
	$1d_{5/2}$	-----	10.859
	$2s_{1/2}$	-----	2.828
^{20}F	$1s_{1/2}$	36.728	40.842
	$1p_{3/2}$	23.553	27.402
	$1p_{1/2}$	20.630	24.503
	$1d_{5/2}$	9.660	13.227
	$2s_{1/2}$	-----	6.601

Fig. 1 shows the $\rho_c(r)$ (black lines), $\rho_v(r)$ (blue lines) and $\rho_m(r)$ (dashed-red lines) for ^{18}N and ^{20}F using the GS (left panel) and WS (right panel) techniques. In this figure, the experimental matter densities (grey region) [22] of ^{18}N and ^{20}F were also plotted. The top and bottom figures represent the densities of ^{18}N and ^{20}F, consecutively. The dashed-red lines and grey region for selected nuclei have a very good agreement, as illustrated in these figures. Furthermore, the dashed-red curves indicate that these nuclei have expanded matter distributions.

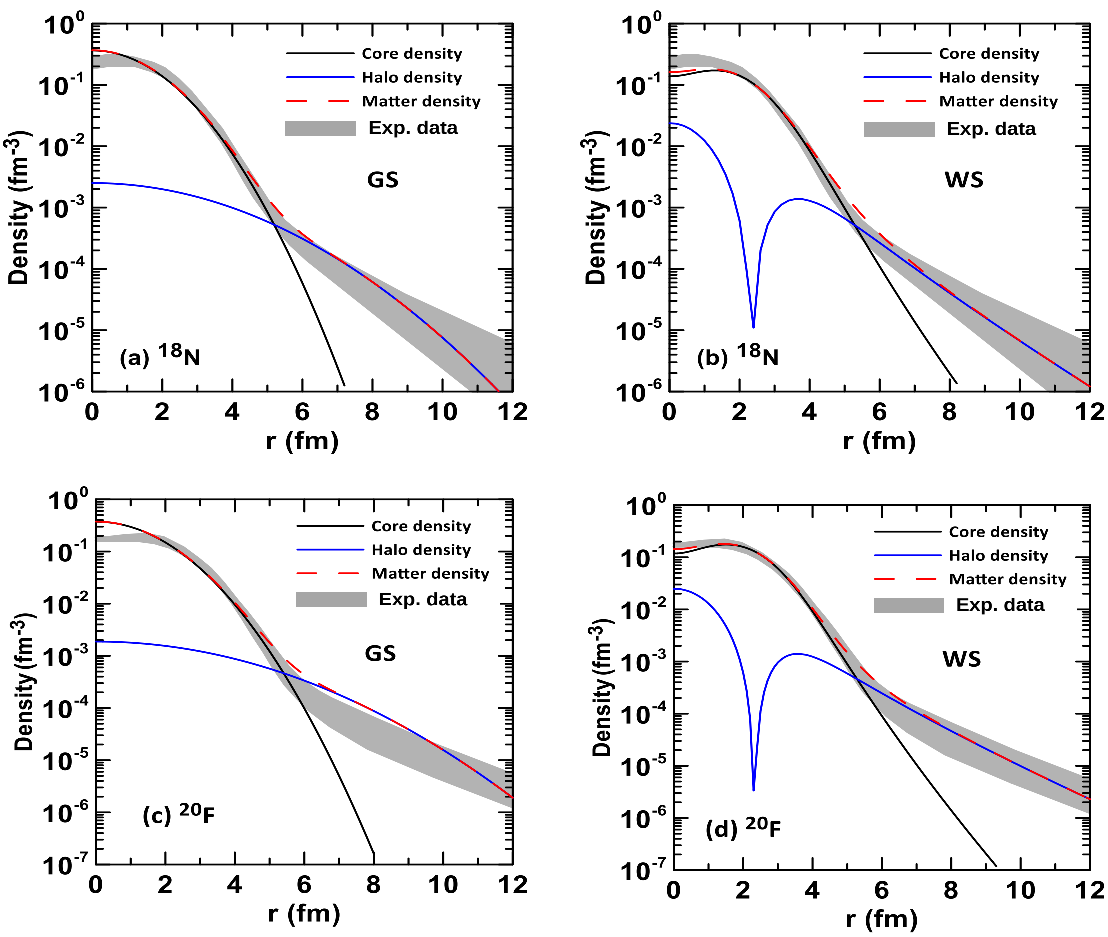

Figure 1: The $\rho_c(r)$, $\rho_v(r)$ and $\rho_m(r)$ distributions for ^{18}N and ^{20}F halo nuclei.

Fig. 2 shows the $\rho_p(r)$ (blue lines), $\rho_n(r)$ (black lines), and $\rho_m(r)$ (dashed-red lines) for ^{18}N (top figures) and ^{20}F (bottom figures). The $\rho_n(r)$ distributions in this figure clearly show the typical behavior of an exotic nucleus (i.e. long-tail property).

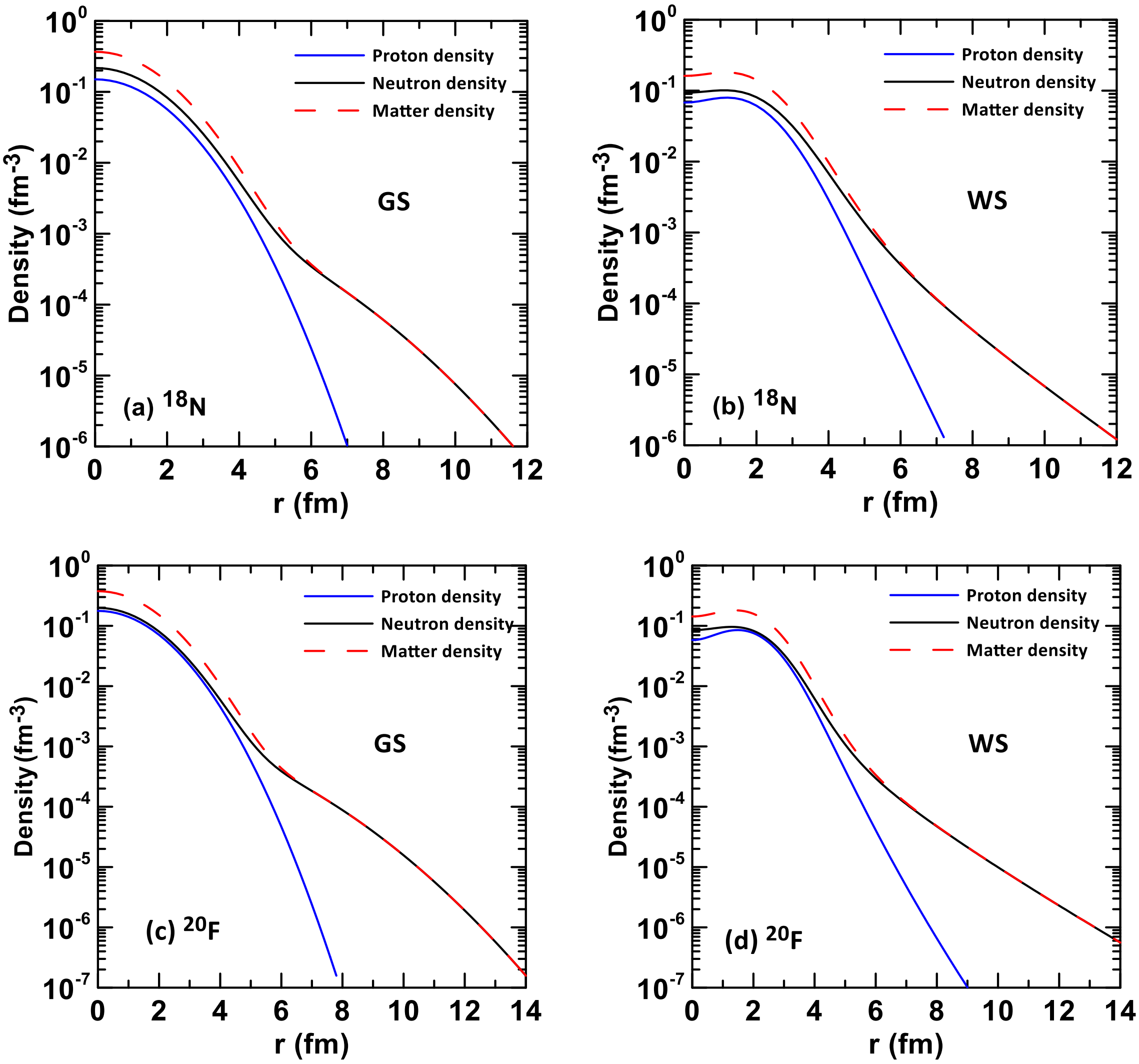

Figure 2: The $\rho_n(r)$, $\rho_p(r)$ and $\rho_m(r)$ distributions for ^{18}N and ^{20}F.

Fig. 3 demonstrates the $\rho_m(r)$ for ^{19,20}F and ^{14,18}N nuclei. The dashed-red and blue lines, respectively, refer to the $\rho_m(r)$ for unstable (^{18}N, ^{20}F) and stable (^{14}N, ^{19}F) nuclei. The blue and dashed-red lines are obviously different, as shown in these figures. The dashed-red lines have a longer tail than the blue lines because the last neutron in ^{18}N and ^{20}F is weakly bonded.

Theoretical C0 form factors for ^{18,14}N Fig. 4(a) and ^{20,19}F Fig. 4(b) calculated by PWBA within proton densities obtained by the WS potential are shown in Fig. 4. The black and red curves respectively, correspond to the C0 of unstable (^{18}N, ^{20}F) and stable (^{14}N, ^{19}F) nuclei. The experimental results of stable nuclei ^{14}N [23] and stable ^{19}F [24] are displayed as blue-dotted symbols for comparison. According to these results, each of the black and red curves has only one diffraction minimum. In comparison to the minimum of ^{14}N [^{19}F], the minimum position of ^{18}N [^{20}F] has an outward [inward] shift. The variation in the $\rho_p(r)$ due to the presence of the extra neutrons in ^{18}N and ^{20}F led to this major difference between the elastic form factors of unstable (exotic) nuclei and their stable isotopes.

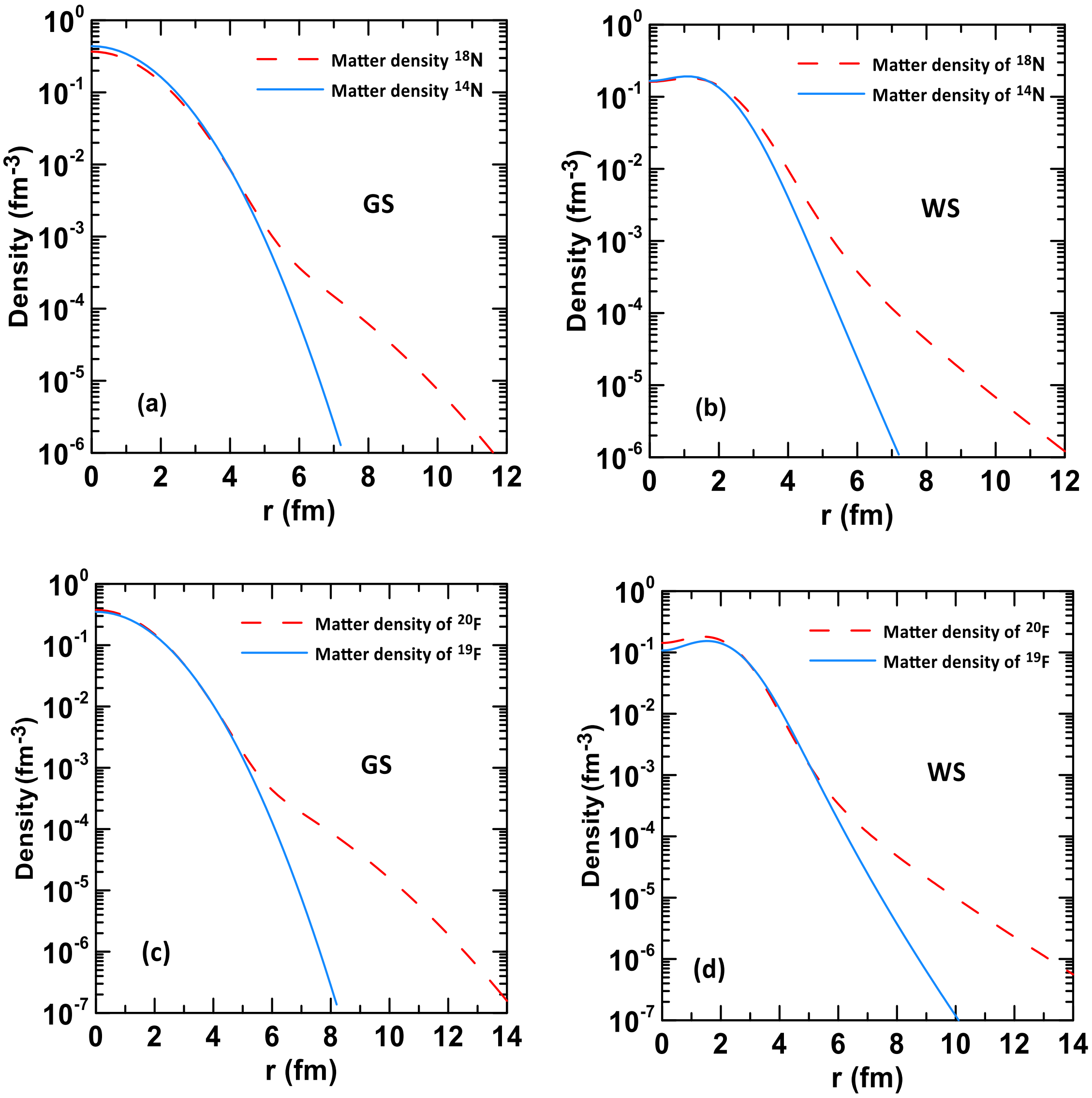

Figure 3: The $\rho_m(r)$ distributions for ^{14,18}N and ^{19,20}F nuclei.

The Kox formula and Glauber model with an OLA were used to compute the σ_R of ^{18}N and ^{20}F on the ^{12}C-target and the results are reported in Table 5 along with the experimental data [20]. The obtained results of σ_R are in good agreement with experimental data, as seen in Table 5.

Fig. 5 shows the dependence of the σ_R calculated via the GM (blue line) on the rms radius to compute the matter rms radius of ^{18}N and ^{20}F from σ_R. The experimental σ_R is shown by the horizontal red line, with the error bar represented by the shaded area. The obtained matter rms radius ($< r_m^2 >^{1/2}$) for the exotic nuclei is represented by the intersection point of the blue line with the horizontal red line. The computed ($< r_m^2 >^{1/2}$) for ^{18}N and ^{20}F are 2.67 and 2.73 fm, respectively, as shown in Fig.5, which matches well with the equivalent experimental results of the values 2.69 $\pm$ 0.05 and 2.79 $\pm$ 0.03 fm [21], respectively.

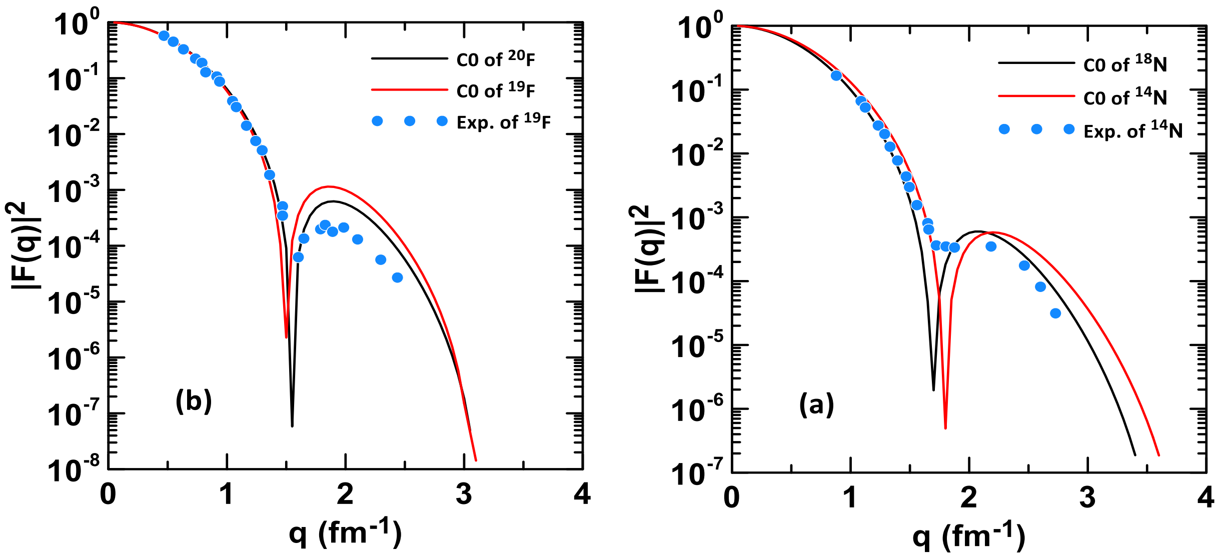

Figure 4: The C0 form factors for ^{14,18}N and ^{19,20}F.

Table 5: The σ_R of ^{18}N and ^{20}F on ^{12}C-target.

Halo nuclei	Energy (MeV) [20]	σ_R (Cal.) (mb)		σ_R (Exp.) (mb) [20]
		Kox formula	GM	
^{18}N	1020	1.053	1047	1046 ±8
^{20}F	950	1118	1015	1113 ±11

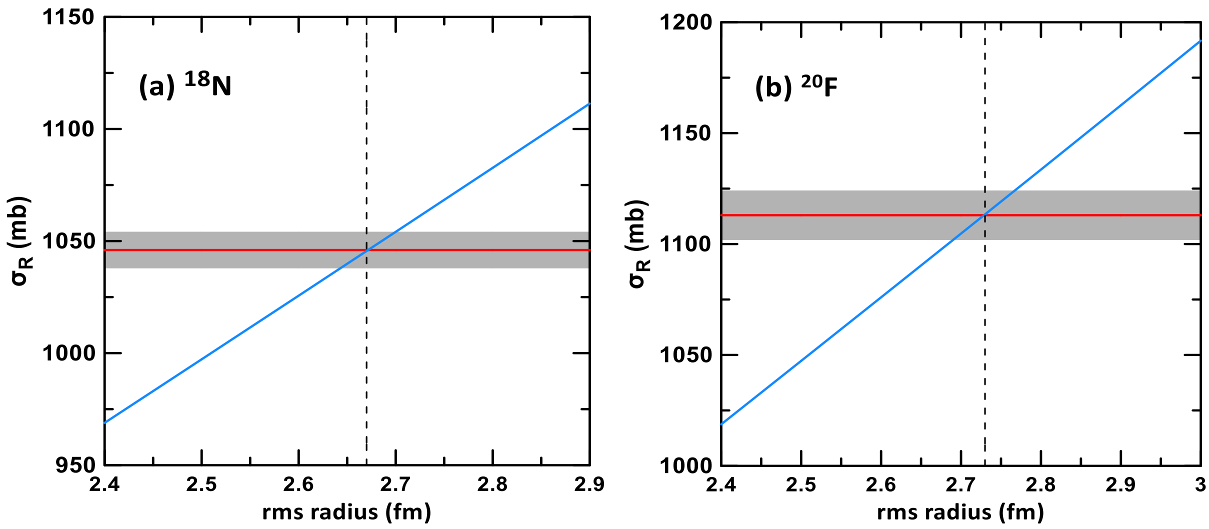

Figure 5: The dependence of the σ_R on the rms radius for ^{18}N and ^{20}F.

4. Conclusions

The GS and WS wave functions within the TBM of [Core + n] were utilized to investigate the ground-state characteristics of halo ^{18}N and ^{20}F nuclei, including $\rho_n(r)$, $\rho_p(r)$ and $\rho_m(r)$ distributions and related rms radii. According to the calculated results, the TBM provides a good description of the nuclear structure for the above neutron-rich exotic nuclei. The PWBA was used to calculate the elastic form factors of exotic nuclei ^{18}N and ^{20}F as well as their stable isotopes ^{14}N and ^{19}F.

The variation in the $\rho_p(r)$ due to the presence of the extra neutrons in ^{18}N and ^{20}F leads to a major difference between the elastic form factors of exotic nuclei and their stable isotopes. The σ_R for these nuclei was investigated using the Kox formula and OLA of GM with single-particle HO wave functions. Furthermore, the GM was employed to calculate the exotic nucleus matter rms radii. The calculated results for the selected exotic nuclei were in good agreement with the experimental data.

Acknowledgements

The authors would like to thanks the Department of Physics, College of Science, University of Baghdad for their help during the research work.

Conflict of Interest

The authors declare that they have no conflicts of interest.

References

1. Saeed E.F. and Flaiyh G.N., *Theoretical study of nuclear density distributions and elastic electron scattering form factors of some proton halo nuclei (^{17}Ne and ^{8}B).* Iraqi Journal of Science, 2018. **59**(2B): pp.847-855.
2. Korolev G., Dobrovolsky A., Inglessi A., Alkhazov G., Egelhof P., Estradé A., Dillmann I., Farinon F., Geissel H., and Ilieva S., *Halo structure of ^{8}B determined from intermediate energy proton elastic scattering in inverse kinematics*. Physics Letters B, 2018. **780**: pp.200-204.
3. Dobrovolsky A., Korolev G., Inglessi A., Alkhazov G., Colò G., Dillmann I., Egelhof P., Estradé A., Farinon F., and Geissel H., *Nuclear-matter distribution in the proton-rich nuclei ^{7}Be and ^{8}B from intermediate energy proton elastic scattering in inverse kinematics*. Nuclear Physics A, 2019. **989**: pp.40-58.
4. Allami A.A. and Alzubadi A.A., S*tudy of the nuclear structure of some exotic nuclei using nonrelativistic and relativistic mean-field methods*. International Journal of Modern Physics E, 2020. **29**(12): pp.1-19.
5. Rahi S.A. and Flaiyh G.N., *Matter density distributions, root-mean square radii and elastic electron scattering form factors of some exotic nuclei (^{17}B, ^{11}Li, ^{8}He).* Iraqi Journal of Physics, 2021. **19**(50): pp.60-69.
6. Antonov A., Kadrev D., Gaidarov M., de Guerra E.M., Sarriguren P., Udias J., Lukyanov V., Zemlyanaya E., and Krumova G., *Charge and matter distributions and form factors of light, medium, and heavy neutron-rich nuclei*. Physical Review C, 2005. **72**(4): pp.1-26.
7. Wen-Jun G., Huan-Qing J., Jian-Ye L., Wei Z., Zhong-Zhou R., and Xi-Guo L., *Total nuclear reaction cross section induced by halo nuclei and stable nuclei*. Communications in Theoretical Physics, 2003. **40**(5): pp.577-584.
8. Alsajjad A.Y.A. and Abdullah A.N., *Density distributions of exotic ^{17}F and ^{19}C nuclei studied by the two-body model*. Diyala Journal For Pure Science, 2019. **15**(04): pp. 120-135.
9. Abdullah A.N., *Nuclear structure investigation of some neutron-rich halo nuclei*. International Journal of Modern Physics E, 2017. **26**(07): pp.1-11.
10. Abdullah A.N., *Investigation of halo structure of neutron rich ^{14}B, ^{15}C, ^{19}C and ^{22}N nuclei in the two body model*. International Journal of Modern Physics E, 2020. **29**(03): pp.1-10.
11. Abdullah A., *Elastic electron scattering from ^{12}Be and framework of the three-body model address for correspondence*. Indian Journal Of Natural Sciences, 2018. **8**: pp.13898.

12. Sallh G.M., *Study of the nuclear structure of halo nuclei ^{23}O and ^{24}F using the two-body model.* Iraqi Journal of Physics, 2020. **18**(46): pp.29-38.
13. Abdullah S.Q. and Abdullah A.N., *Matter density distributions and reaction cross sections for ^{8}Li and ^{22}N exotic nuclei*. Iraqi Journal of Science, 2022. **63**(3): pp.1030-1038.
14. Antonov A., Gaidarov M., Kadrev D., Hodgson P., and De Guerra E.M., *Charge density distributions and related form factors in neutron-rich light exotic nuclei*. International Journal of Modern Physics E, 2004. **13**(04): pp.759-772.
15. Zheng T., Yamaguchi T., Ozawa A., Chiba M., Kanungo R., Kato T., Katori K., Morimoto K., Ohnishi T., and Suda T., *Study of halo structure of ^{16}C from reaction cross section measurement*. Nuclear Physics A, 2002. **709**(1-4): pp.103-118.
16. Tostevin J. and Al-Khalili J., *How large are the halos of light nuclei?* Nuclear Physics A, 1997. **616**(1-2): pp.418-425.
17. Kox S., Gamp A., Perrin C., Arvieux J., Bertholet R., Bruandet J., Buenerd M., Cherkaoui R., Cole A., and El-Masri Y., *Trends of total reaction cross sections for heavy ion collisions in the intermediate energy range*. Physical Review C, 1987. **35**(5): pp.1678-1691.
18. Audi G., Wapstra A., and Thibault C., *The Ame2003 atomic mass evaluation:(ii). tables, graphs and references.* Nuclear physics A, 2003. **729**(1): pp. 337-676.
19. Kondev F., Wang M., Huang W., Naimi S., and Audi G., *The nubase 2020 evaluation of nuclear physics properties*. Chinese Physics C, 2021. **45**(3):pp.1-181.
20. Ahmad S., Usmani A., and Khan Z., *Matter radii of light proton-rich and neutron-rich nuclear isotopes*. Physical Review C, 2017. **96**(6): pp.1-13.
21. Ozawa A., Suzuki T., and Tanihata I., *Nuclear size and related topics*. Nuclear Physics A, 2001. **693**(1-2): pp.32-62.
22. Ozawa A., *Measurement of the interaction cross-section and related topics*. The European Physical Journal A-Hadrons Nuclei, 2002. **13**(1): pp.163-167.
23. Dally E., Croissiaux M., and Schweitz B., *Scattering of high-energy electrons by nitrogen-14 and-15*. Physical Review C, 1970. **2**(6): pp.2057-2068.
24. Hallowell P., Bertozzi W., Heisenberg J., Kowalski S., Maruyama X., Sargent C., Turchinetz W., Williamson C., Fivozinsky S., and Lightbody Jr J., *Electron scattering from ^{19}F and ^{40}Ca*. Physical Review C, 1973. **7**(4): pp.1396-1409.

عوامل التشكل المرنة وتوزيعات الكثافة المادية لبعض النوى الغنية بالنيوترونات

حوراء كاظم مهدي[1] و أحمد نجم عبدالله[1]
[1]قسم الفيزياء، كلية العلوم، جامعة بغداد، بغداد، العراق

الخلاصة
تم دراسة خصائص الحالة الارضية مثل توزيعات الكثافة النيوترونية، البروتونية والمادية وانصاف الاقطار النووية للنوى الغريبة ^{18}N و ^{20}F باستخدام أنموذج الجسيمين مع الدوال الموجية لجهدي كاوس وودز- ساكسون. تم الحصول على خاصية الامتداد الطويل في توزيعات الكثافة النيوترونية والمادية لهذه النوى. تم استخدام تقريب بورن للموجة المستوية لدراسة عوامل التشكل المرنة لهذه النوى. ان التباين في توزيعات الكثافة البروتونية نتيجة وجود النيوترونات الإضافية في النوى ^{18}N و ^{20}F أدى الى الاختلاف بين عوامل التشكل لهذه النوى الغريبة ونظيرتها المستقرة ^{14}N و ^{19}F. المقاطع العرضية للتفاعل لهذه النوى تمت دراستها باستخدام أنموذجي كوكس وجلوبر. بالإضافة الى ذلك تم استخدام انموذج جلوبر لحساب انصاف الاقطار النووية المادية لهذه النوى تم دراستها باستخدام. النتائج المحسوبة لانصاف الأقطار النووية تتفق بشكل جيد مع القيم العملية.